A&A 404, 449–463 (2003)
DOI: 10.1051/0004-6361:20030493

Astronomy & Astrophysics

Photoionized O VI absorbers toward the bright QSO HE 0515–4414⋆

S. A. Levshakov[1], I. I. Agafonova[1], D. Reimers[2], and R. Baade[2]

[1] Department of Theoretical Astrophysics, Ioffe Physico-Technical Institute, 194021 St. Petersburg, Russia
[2] Hamburger Sternwarte, Universität Hamburg, Gojenbergsweg 112, 21029 Hamburg, Germany

Received 20 December 2002 / Accepted 31 March 2003

Abstract. We report on detailed Monte Carlo inversion analysis of five O VI systems from the spectrum of the bright quasar HE 0515–4414 ($z_{\rm em} = 1.71$). The associated system at $z_{\rm abs} = 1.697$ with the neutral hydrogen column density $N({\rm H\,I}) = 4.4 \times 10^{13}$ cm^{-2} shows pronounced absorption from highly ionized transitions of C III, C IV, N V, O VI, Si IV, and probably S VI. We found that only a power law type ionizing spectrum ($J_\nu \propto \nu^{-1.5}$) is consistent with the observed sample of the line profiles, i.e. the system is definitely intrinsic. The relative metal abundances give almost the solar pattern and the metallicity of ∼5 times solar. The system originates in a thin shell of the line-of-sight thickness $L \lesssim 16$ pc. Two O VI systems at $z_{\rm abs} = 1.674$ ([C/H] $\simeq -1.6$) and 1.602 ([O/H] $\simeq -1.1$), arising in intervening halos, have linear sizes of $L \simeq 3$–14 kpc and ≃17 kpc, respectively. Absorption systems at $z_{\rm abs} = 1.385$ ([C/H] $\simeq -0.3$, $L \simeq 1.7$–2.5 kpc) and $z_{\rm abs} = 1.667$ ([C/H] $\simeq -0.5$, $L \simeq 1$ kpc) exhibit characteristics very similar to that observed in metal-enriched high velocity clouds in the Milky Way. These systems are probably embedded in extremely metal-poor halos with [C/H] < -2.4 ($z_{\rm abs} = 1.667$) and [C/H] < -3.7 ($z_{\rm abs} = 1.385$). We also found two additional extremely metal-poor Lyα systems at $z_{\rm abs} = 1.500$ and 1.681 with, respectively, $N({\rm H\,I}) \simeq 1.7 \times 10^{15}$ and 1.8×10^{15} cm^{-2} and [C/H] < -4.0 and < -3.0, – an indication that the distribution of metals in the metagalactic medium is utterly patchy. Our results show that the ionization states in the analyzed O VI absorbers, ranging from $z \simeq 1.4$ to 1.7, can be maintained by photoionization only and that the fraction of the shock-heated hot gas with temperature $T_{\rm kin} > 10^5$ K is negligible in these systems.

Key words. cosmology: observations – line: formation – line: profiles – quasars: absorption lines – quasars: individual: HE 0515–4414

1. Introduction

In recently published paper, Reimers et al. (2001, hereafter RBHL) reported on the identification of six O VI absorption systems in the redshift range $1.38 < z < 1.73$ found in the light of the luminous quasar HE 0515–4414, $z_{\rm em} = 1.71$, $V = 14.9$ (Reimers et al. 1998). Here we present the physical parameters and metal abundances for four of these systems and for a fifth new one. The analysis was performed with the Monte Carlo inversion (MCI) algorithm which is described in detail in our previous publications (Levshakov et al. 2000, hereafter LAK; Levshakov et al. 2002). Since this technique is relatively new, we briefly outline its basics below.

The main assumption of the MCI procedure is that all lines observed in an intervening absorption system arise in a *continuous* absorbing gas slab of a thickness L with a fluctuating gas density and a random velocity field. The metal abundances within the absorber are constant (the validity of this assumption is discussed in Levshakov et al. 2003a), the gas is in the thermal and ionization equilibrium, and it is optically thin in the ionizing background radiation. The intensity and the shape of the photoionizing radiation are considered as external parameters.

Within the absorbing region the radial velocity $v(x)$ and the total volumetric gas density $n_{\rm H}(x)$ along the line of sight are considered as two continuous random functions represented by their sampled values at equally spaced intervals Δx. The computational procedure is based on the adaptive simulated annealing. Fractional ionizations of different elements are calculated at every space coordinate x with the photoionization code CLOUDY (Ferland 1997).

Using the MCI, we estimate the following physical characteristics of the intervening gas cloud: the mean ionization parameter U_0, the total hydrogen column density $N_{\rm H}$, the line-of-sight velocity and density dispersions of the bulk material ($\sigma_{\rm v}$ and $\sigma_{\rm y}$, respectively), and the chemical abundances $Z_{\rm a}$ of all elements involved in the analysis. With these parameters we can further calculate the mean gas number density n_0, the column densities for different species $N_{\rm a}$, the mean kinetic temperature $T_{\rm kin}$, and the linear size L. This comprehensive

Send offprint requests to: S. A. Levshakov,
e-mail: lev@astro.ioffe.rssi.ru

⋆ Based on observations with the NASA/ESA Hubble Space Telescope, obtained at the Space Telescope Science Institute, which is operated by Aura, Inc., under NASA contract NAS 5-2655; and on observations collected at the VLT/Kueyen telescope ESO (Paranal, Chile), under programme ID 066.A-0212.

information makes it possible to classify the absorber more reliably and hence to obtain important clues concerning the physical conditions in the high redshift objects.

While interpreting results of the MCI, the following should be taken into account. For every point within the line profile the observed intensity results from a *superposition* of different ionization states (for details, see Fig. 1 in LAK). The value of the mean ionization parameter U_0 is related to the parameters of the gas cloud as (see Eq. (28) in LAK)

$$U_0 = \frac{n_{\rm ph}}{n_0}\left(1+\sigma_{\rm y}^2\right). \quad (1)$$

Here $n_{\rm ph}$ is the number density of photons with energies above 1 Ryd which is determined by

$$n_{\rm ph} = \frac{4\pi}{ch} J_{912} \int_{\nu_{\rm c}}^{\infty} \left(\frac{J_\nu}{J_{912}}\right) \frac{{\rm d}\nu}{\nu}\ , \quad (2)$$

where $c, h, \nu_{\rm c}$, J_ν, and J_{912} are, respectively, the speed of light, the Planck constant, the frequency of the Lyman limit, the mean specific intensity of the radiation background averaged over all lines of sight, and the mean specific intensity at the hydrogen Lyman edge (in units of erg cm^{-2} s^{-1} Hz^{-1} sr^{-1}).

Equation (1) shows that if the density field is fluctuating ($\sigma_{\rm y} > 0$), then with the same mean density n_0 and the same background ionizing spectrum a higher value of U_0 can be realized without any additional sources of ionization. Intermittent regions of low and high ionization caused by the density fluctuations will occur in this case along the line of sight leading to a lower value of the total hydrogen column density $N_{\rm H}$ as compared with a homogeneous gas slab model ($\sigma_{\rm y} = 0$). On the other hand, for a given U_0 the mean gas density n_0 is also higher in fluctuating media. Since $L = N_{\rm H}/n_0$, the value of the linear size calculated under the assumption of a fluctuating gas density is much smaller as compared to that obtained for a model of a constant gas density.

One of the problems in the interpretation of the O VI absorbers is a high overabundance of oxygen compared to other elements, in particular, to carbon and especially to silicon (e.g. Carswell et al. 2002) which is obtained from the photoionization models assuming a homogeneous gas density. It is well known that the metal abundances measured in the absorption systems depend in a crucial way on the adopted spectral shape of the ultraviolet background ($\lambda < 912$ Å). A mean metagalactic spectrum of the UV radiation as a function of z may be estimated from theoretical calculations (e.g., Haardt & Madau 1996, hereafter HM; Fardal et al. 1998), but for every particular system one can never exclude that the shape of this spectrum is affected by local sources (see, e.g., Reimers et al. 1997; Kriss et al. 2001; Smette et al. 2002). However, if the system contains metal lines of many ions in different ionization stages and the relative abundance ratios of the elements are known either from observations (e.g., in galaxies or stars) or from theoretical calculations of stellar nucleosynthetic yields, then it is possible to restore the spectral shape of the ionizing continuum responsible for the ionization states in a system under study. We used this approach in the present work while analyzing the absorption systems at $z_{\rm abs}$ = 1.385, 1.602, 1.667, 1.674, and 1.697.

The structure of the paper is as follows. The observations are described in Sect. 2. Physical states of the O VI absorption systems are outlined in Sect. 3. Notes on individual O VI absorbers are given in Sect. 4. The obtained results are discussed in Sect. 5, and we draw our conclusions in Sect. 6.

2. Observations

Observations and data reduction are described in detail in RBHL. Here we list the main characteristics of the data obtained which are relevant to the present study.

HE 0515–4414 was observed with the HST/STIS in January and February 2000, with the medium resolution NUV echelle mode (E230M) and a 0.2×0.2 aperture which provides a resolution of ∼30 000 (*FWHM* ≃ 10 km s^{-1}). The spectrum covers the range between 2279 Å and 3080 Å where the moderate *S/N* ratio (between 10 and 20 per resolution element) is achieved.

Echelle spectra of HE 0515–4414 were obtained during ten nights between October 7, 2000 and January 2, 2001 using the UV-Visual Echelle Spectrograph (UVES) installed at the VLT/Kueyen telescope. These observations were carried out under good seeing conditions (0.47–0.70 arcsec) and a slit width of 0.8 arcsec giving the spectral resolution of ∼55 000 (*FWHM* ≃ 6 km s^{-1}). The VLT/UVES data have very high *S/N* ratio (between 50 and 100 per resolution element) which allows us to detect very weak absorption features.

The observed wavelength scales for both sets of data were transformed into vacuum heliocentric wavelengths. The calibrated spectra were added together using weights proportional to their *S/N*.

3. O VI absorption in photo- and shock-heated gas

The observation and interpretation of the extragalactic O VI absorption systems is closely linked to cosmological simulations of hierarchical structure formation which predict that a substantial fraction of intergalactic gas is shock-heated to high temperatures ($T_{\rm kin} \sim 10^5$–10^7 K) at low redshift and that a considerable fraction of baryons (up to ∼50%) resides in this "warm-hot" gas phase at $z = 0$. With increasing redshift, the fraction of baryons decreases rapidly (down to ∼5%) at $z = 3$ (e.g., Cen & Ostriker 1999; Davé et al. 2001). Recently obtained results indicate that the cosmological mass density of the low-z O VI systems may be comparable to the combined cosmological mass density of stars and cool gas in galaxies and X-ray gas in galaxy clusters at low z (Tripp et al. 2000).

The interpretation of the O VI lines is not, however, straightforward, especially when we are dealing with high-z systems. The resonance line doublet of O VI may arise in both collisionally ($T > 10^5$ K) and photoionized ($T \sim 10^4$ K) gas. Moreover, the absorbing region may be not homogeneous, a gas slab may be exposed to a time-dependent source of ionizing radiation, and what we observe may be a mixture of different phases, which may not be in ionization equilibrium (e.g., regions behind shock fronts).

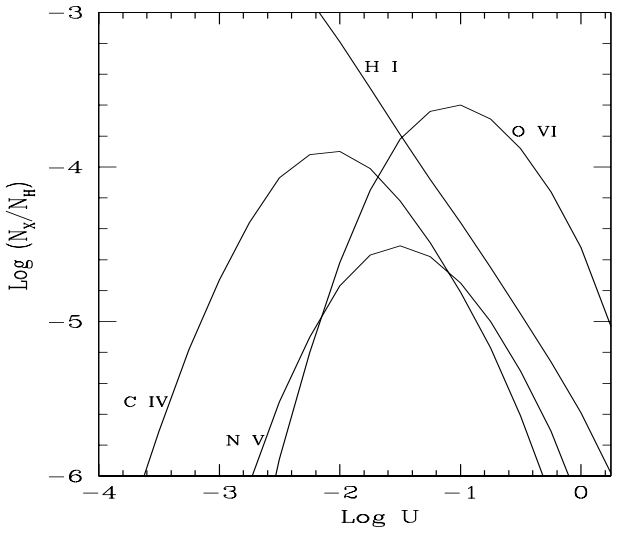

Fig. 1. Relative column densities (in units of the total hydrogen column density $N_{\rm H}$) plotted as a function of the ionization parameter U for a highly ionized gas in photoionization equilibrium (the UV background field $\propto \nu^{-1.5}$). Photospheric solar abundances from Grevesse & Sauval (1998) are used.

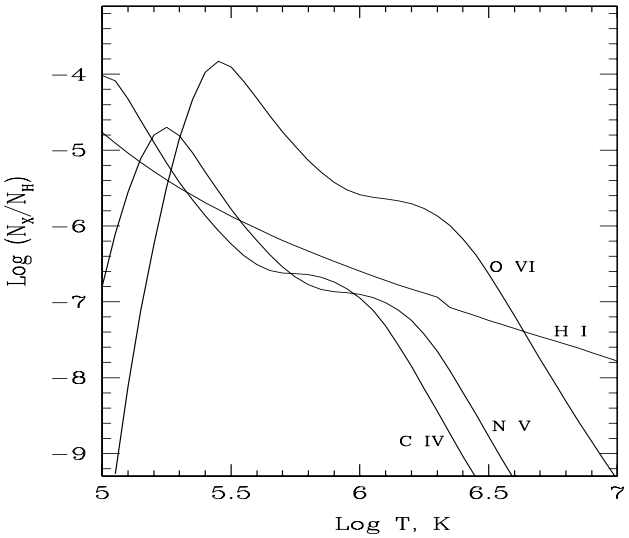

Fig. 2. Relative column densities (in units of the total hydrogen column density $N_{\rm H}$) plotted as a function of the temperature T for a highly ionized gas in collisional ionization equilibrium. Photospheric solar abundances from Grevesse & Sauval (1998) are used.

To outline the main characteristics of an absorption system arising in the collisionally or radiatively ionized gas, it is, however, worthwhile to consider an equilibrium situation. A non-equilibrium case should lie between the results obtained for collisional or radiative equilibrium. In this regard, it is very illustrative to compare column densities of the most abundant ions calculated for a simplified model of a plane parallel gas slab that is either in photoionization equilibrium in a radiation field or in collisional equilibrium at a given temperature T. The gas is assumed to be optically thin in the ionizing Lyman continuum.

If we define $N_{{\rm a},i}$ as the total ion column density of element "a" in the ith ionization stage ($N_{\rm a} = \sum_i N_{{\rm a},i}$) and $\Upsilon_{{\rm a},i} = N_{{\rm a},i}/N_{\rm a}$ as the fractional ionization of ions {a, i}, then their relative column density in units of the total hydrogen column density $N_{\rm H}$ is given by

$$N_{{\rm a},i}/N_{\rm H} = Z_{\rm a}\,\Upsilon_{{\rm a},i}\,, \qquad (3)$$

where $Z_{\rm a}$ is the metal abundance.

Figures 1 and 2 show the relative column densities of H I, C IV, N V, and O VI (for illustration, solar abundances are used) plotted against the ionization parameter U for the photoionization caused by the power law background $J_\nu \propto \nu^{-1.5}$ (calculated with CLOUDY), and against T for the collisional ionization case (the ionization fractions are from Sutherland & Dopita 1993). In both cases O VI dominates for high excitation conditions. The photoionization equilibrium is characterized by strong hydrogen lines in the range $\log U \lesssim -1$ where all metal absorptions can be observed simultaneously. In collisional ionization equilibrium Lyα is much weaker in the range $5.5 \lesssim \log(T) \lesssim 6.0$ where O VI is the most readily observed ion in the ultraviolet range. At these temperatures, other lines (C IV and/or N V) are also very weak and hardly observable in real spectra. Indeed, if we assume an absorber of $N_{\rm H} = 10^{18}$ cm^{-2}, then at $T_{\rm kin} = 3 \times 10^5$ K the central optical depths of these species and their Doppler b-parameters are as follows: $\tau_0({\rm Ly}\alpha) = 0.014$, $b_{{\rm Ly}\alpha} = 73$ km s^{-1}; $\tau_0({\rm C\,IV}_{1548}) = 0.012$, $b_{\rm C\,IV} = 21$ km s^{-1}; $\tau_0({\rm N\,V}_{1238}) = 0.015$, $b_{\rm N\,V} = 20$ km s^{-1}; and $\tau_0({\rm O\,VI}_{1031}) = 1.40$, $b_{\rm O\,VI} = 18$ km s^{-1}.

For the abundances different from the solar values the estimated optical depths of the metal lines can be scaled correspondingly using Eq. (3) and the curves from Fig. 2.

4. Results on individual O VI systems

In this section we consider O VI systems observed in the spectrum of HE 0515–4414. All physical parameters listed below in Table 1 were derived using the MCI procedure as described in LAK. The internal errors of the fitting parameters $U_0, N_{\rm H}, \sigma_{\rm v}, \sigma_{\rm y}$ and $Z_{\rm a}$ are about 15%–20%, the errors of the measured column densities are less than 5% for the high *S/N* UVES data and of about 15%–25% for the moderate *S/N* STIS spectra. It should be noted that the errors of the fitting parameters reflect merely the configuration of the parameter space in the vicinity of a minimum of the objective function (this function is defined by Eqs. (29) and (30) in LAK). To what extent the recovered parameters may correspond to their real values is discussed separately for each individual absorption system.

In some systems with rather high neutral hydrogen column densities [N(H I) $\sim 10^{15}$ cm^{-2}] we did not detect any transitions of high or low most abundant ions in the observational range from 2279 Å to 6662 Å. We will call such systems formally as "metal-free" throughout the text with all reserve for a probability that they may contain transitions in the far UV-range like O IV λ554.1, O V λ629.7, O VII λ21.6, O VIII λ19.0 or Ne VII λ465.2, and Ne VIII λ770.4 Å. The upper limits on the column densities of ions from the observational range were

calculated in the following way. We define the equivalent width detection limit, $\sigma_{\rm lim}$, as (Levshakov et al. 1992):

$$\sigma_{\rm lim} = \Delta\lambda \left(\langle S/N \rangle^{-2} \mathcal{M} + \delta_c^2 \mathcal{M}^2 \right)^{1/2} \quad . \tag{4}$$

Here $\langle S/N \rangle$ is the mean signal-to-noise ratio at the expected position of an absorption line, $\delta_c = \sigma_c / C$ is the accuracy of the local continuum fit over the width of the line, $\mathcal{M} = 2.5{\times}FWHM$ is the full width (in pixels) at the continuum level of a weak absorption line, and $\Delta\lambda$ is the pixel size in Å. In calculations we used $\mathcal{M} = 10$, i.e. $\Delta\lambda/\lambda = \frac{1}{4} FWHM/c$.

Equation (4) shows that the minimum detectable equivalent width, defined as $W_{\rm lim} = 3\,\sigma_{\rm lim}$, is very sensitive to the accuracy of the continuum fitting, and $W_{\rm lim}$ increases as the data become more noisy.

For a weak absorption line ($\tau_0 \ll 1$) the column density does not depend on the broadening parameter b and is proportional to $W_{\rm lim}$:

$$N_{\rm lim} = 1.13 \times 10^{20} \, \frac{W'_{\rm lim}}{\lambda_0^2 \, f} \, {\rm cm}^{-2} \, , \tag{5}$$

where f is the oscillator strength for the absorption transition, λ_0 is the line-center rest wavelength in Å, and $W'_{\rm lim}$ is the rest-frame equivalent width. Using this linear approximation to the curve of growth, we calculated the upper limits $N_{\rm lim}$ listed in Table 2 (absorption lines used in this analysis are listed in Col. 2). The values of λ_0 and f were taken from Morton (1991) and from Spitzer & Fitzpatrick (1993) for the Si II λ1526.7 Å line.

We also note that the quasar HE 0515–4414, being the brightest known QSO at $z > 1.5$, has the absolute magnitude $M \simeq -30$ (assuming $\Omega = 1$ and $H_0 = 75$ km s^{-1} Mpc^{-1}) and, thus, its luminosity is $\mathcal{L}_{\rm Q} \simeq 2.5 \times 10^{47}$ erg s^{-1}. Three O VI systems – that at $z_{\rm abs} = 1.667$, 1.674 and 1.697 – are not far from the QSO emitting region ($\Delta v_{\rm em-abs} \simeq 4760, 4000$ and 1500 km s^{-1}, respectively), and hence the intensity of the incident continuum emitted by the quasar may exceed the value of a mean intensity of the background ionizing radiation at the positions of these absorbers. According to HM, the Lyman-limit specific intensity J_{912} of the metagalactic field at $z \simeq 1.6$–1.8 is about 0.5×10^{-21} erg cm^{-2} s^{-1} Hz^{-1} sr^{-1}. If the velocity differences $\Delta v_{\rm em-abs}$ are caused entirely by the cosmological expansion, then the proper luminosity distances between the QSO and the absorbers at $z_{\rm abs} = 1.667$, 1.674 and 1.697 are $14.6\,h_{75}^{-1}$ Mpc, $12.2\,h_{75}^{-1}$ Mpc and $4.3\,h_{75}^{-1}$ Mpc, respectively, and the corresponding local Lyman-limit specific intensities due to the QSO at $z = 1.67$ is $J_{\rm Q} \simeq 2.0 \times 10^{-21}$ erg cm^{-2} s^{-1} Hz^{-1} sr^{-1} and $J_{\rm Q} \simeq 1.0 \times 10^{-20}$ erg cm^{-2} s^{-1} Hz^{-1} sr^{-1} at $z = 1.70$ (assuming a single power law spectrum for the quasar continuum at $\lambda < 912$ Å with the spectral index $\alpha = -1.5$). The value of $J_{\rm Q}$ becomes comparable with J_{912} only for the $z_{\rm abs} = 1.602$ system where $J_{\rm Q} \simeq 0.3 \times 10^{-21}$ erg cm^{-2} s^{-1} Hz^{-1} sr^{-1}. These estimated $J_{\rm Q}$ values were used to calculate the mean densities n_0 and linear sizes L of the O VI systems.

In our study we used different ionizing background spectra, some of which are shown in Fig. 3. For every system, we started calculations with a HM spectrum, and if it failed to reproduce self-consistently the observational data another types of photoionizing continua were tested.

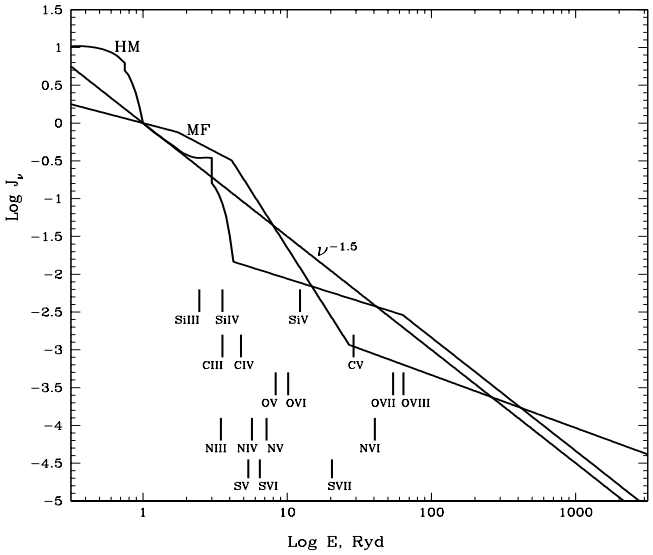

Fig. 3. UV-background ionizing continua used in the present calculations. The spectra have been normalized so that $J_\nu(h\nu = 1\ {\rm Ryd}) = 1.0$. Shown are: HM – a mean metagalactic spectrum at $z = 2$ with a decrement at 4 Ryd to account for He II attenuation in intervening Lyα clouds as computed by Haardt & Madau (1996); MF – an AGN type spectrum deduced by Mathews & Ferland (1987), and $\nu^{-1.5}$ – a single power law spectrum $J_\nu \propto \nu^{-1.5}$. The positions of ionization thresholds of different ions are indicated by tick marks.

4.1. O VI absorber at $z_{\rm abs} = 1.697$

The system exhibits a wealth of ions. Namely, at $N({\rm H\,I}) = 4.4 \times 10^{13}$ cm^{-2} (see Table 1) we observe absorption lines of C III, C IV, N V, O VI, Si IV, and probable S VI (as far as we know the ion S VI has never been observed in low H I column density systems at high redshift). Besides, there are continuum "windows" at the positions of the C II 1334 Å, Si II 1260 Å, N III 989 Å, and Si III 1206 Å lines which can be used to constrain the ionization state in the cloud. Thus we can expect that the ionization corrections and, hence, the metal abundances for all elements will be estimated with a sufficiently high accuracy. This gives us a unique opportunity to restore the shape of the local ionizing continuum if we further take into account the measurements of the relative abundances in spiral and elliptical galaxies. For instance, the abundance ratios of α-elements (in our case Si and S) to oxygen appear to be universally constant and independent on metallicity (Henry & Worthey 1999).

The metal lines in the $z_{\rm abs} = 1.697$ cloud are completely resolved with both STIS and UVES spectral resolutions. The line profiles of different ions at different ionization stages demonstrate similar narrow cores, $FWHM \simeq 20$ km s^{-1}. This fact unambiguously indicates that the turbulent broadening dominates over the thermal one, and as a consequence the kinetic temperature of the gas containing highly ionized ions must be considerably lower than 1.3×10^5 K – the value estimated from the width of the O VI 1037 Å assuming a pure thermal line width. However, even if $T_{\rm kin} = 1.3 \times 10^5$ K, then the ionization fractions of N V and O VI in the collisional ionization equilibrium are $\Upsilon_{\rm N\,V} = 0.034$ and $\Upsilon_{\rm O\,VI} = 1.1 \times 10^{-5}$, respectively (e.g., Spitzer 1978; Sutherland & Dopita 1993).

Table 1. Physical parameters of the O VI systems toward HE 0515–4414 (z_{em} = 1.71) derived by the MCI procedure.

Parameter	z_{abs} = 1.385		z_{abs} = 1.602	z_{abs} = 1.667	z_{abs} = 1.674		z_{abs} = 1.697
(1)	(2)	(3)	(4)	(5)	(6)	(7)	(8)
UV[a]	mHM	HM	HM	$\nu^{-1.5}$	HM	$\nu^{-1.5}$	$\nu^{-1.5}$
U_0	0.11	0.11	0.26	0.20	0.18	0.07	0.06
N_H, cm^{-2}	1.2E18	9.9E17	8.1E18	1.1E18	5.5E19	1.7E19	4.8E17
σ_v, km s^{-1}	18.8	18.8	29.3	14.0	53.7	53.0	19.2
σ_y	0.4	0.5	0.9	0.3	0.9	0.9	0.4
Z_C^b	1.2E-4	9.3E-5	<7.5E-6	7.0E-5	1.8E-6	5.7E-6	1.3E-3
Z_N	<2.1E-5	<2.1E-5	<2.7E-5	1.2E-5	<3.0E-7	<5.0E-7	3.0E-4
Z_O	3.8E-4	4.5E-4	4.4E-5	1.7E-4	1.9E-5	4.1E-5	3.3E-3
Z_{Si}	<3.5E-5	<3.5E-5	...	...	<1.3E-6	<2.0E-6	2.3E-4
Z_S	...	...	...	...	...	...	8.0E-5
$[Z_C]$[c]	-0.31 ± 0.09	-0.42 ± 0.08	<-1.51	-0.54 ± 0.15	-2.13 ± 0.09	-1.63 ± 0.09	0.72 ± 0.08
$[Z_N]$	<-0.61	<-0.61	<-1.51	-0.85 ± 0.15	<-2.41	<-2.21	0.55 ± 0.12
$[Z_O]$	-0.11 ± 0.17	-0.04 ± 0.17	-1.05 ± 0.23	-0.46 ± 0.20	-1.41 ± 0.12	-1.08 ± 0.12	0.83 ± 0.11
$[Z_{Si}]$	<0	<0	...	...	<-1.4	<-1.2	0.84 ± 0.15
$[Z_S]$	...	...	...	...	...	...	0.57 ± 0.15
N(H I), cm^{-2}	5.6E13	5.3E13	1.4E14	2.2E13	9.3E14	1.3E15	4.4E13
N(C III), cm^{-2}	7.0E12	5.5E12	<1.3E12	...	...	...	9.0E12
N(N III), cm^{-2}	...	...	...	...	...	...	<2.1E12
N(Si III), cm^{-2}	...	...	...	...	...	...	<4.0E10
N(C IV), cm^{-2}	1.8E13	1.7E13	<3.5E12	1.4E12	9.1E12	8.2E12	6.8E13
N(Si IV), cm^{-2}	<1.0E11	<1.0E11	...	...	<6.4E10	<7.0E10	2.4E11
N(N V), cm^{-2}	<4.9E12	<4.9E12	<2.9E12	1.4E12	<1.6E12	<1.8E12	4.4E13
N(O VI), cm^{-2}	1.0E14	7.6E13	5.1E13	5.0E13	1.1E14	1.1E14	4.5E14
N(S VI), cm^{-2}	...	...	...	...	...	...	5.7E12
n_0, cm^{-3}	1.5E-4	2.0E-4	1.6E-4	4.1E-4	8.3E-4	2.1E-3	≥1.0E-2[d]
$\langle T_{kin} \rangle$, K	2.5E4	2.3E4	4.3E4	3.3E4	4.5E4	3.7E4	1.9E4
T_{kin}^{min}, K	1.8E4	1.9E4	3.0E4	2.9E4	3.0E4	2.6E4	1.6E4
T_{kin}^{max}, K	2.7E4	2.8E4	5.3E4	3.8E4	7.5E4	5.3E4	2.2E4
L, kpc	2.5	1.7	17	0.9	14	2.7	≤1.6E-2[d]

[a] HM (mHM) is a Haardt-Madau (modified Haardt-Madau) type spectrum (see text).

[b] $Z_X = X$/H, $[Z_X] = \log(Z_X) - \log(Z_X)_\odot$.

[c] errors of $[Z_X]$ include uncertainties in the solar abundances as well.

[d] more probable values of n_0 and L are, respectively, 0.2 cm^{-3} and 0.8 pc as discussed in Sect. 5.

The measured column densities N(N V) = 4.4×10^{13} cm^{-2} and N(O VI) = 4.5×10^{14} cm^{-2} would require a unrealistic oversolar abundance ratio [O/N][1] = 3.74. Thus we can conclude that the fraction of the collisionally ionized gas is negligible in the z_{abs} = 1.697 cloud and that the ionization state within this cloud should be determined by photoionization only.

An attempt to describe this system using a HM ionizing spectrum at $z = 1.7$ gives inconsistent profiles of the C III 977 Å and C IV 1548, 1550 Å lines: the observed amount of C III is much less than the computed one. Moreover, the relative abundance ratio [C/O] was too low: [C/O] < −0.7 which is in clear contradiction with the observations of extragalactic H II regions showing [C/O] ≳ −0.5 (Henry et al. 2000). Thus, the HM spectrum has been ruled out.

Since this system is probably located not far from the quasar, its ionization state can be directly affected by the QSO emission. Unfortunately, the exact shape of the far UV continuum of HE 0515–4414 is not known (it was observed only in the rest frame region $\lambda > 740$ Å, see Reimers et al. 1998). To approximate the ionizing continuum we used several power law type spectra (α ranges from −1.2 to −1.8) as well as an AGN type spectrum deduced by Mathews & Ferland (1987, hereafter MF). The MF continuum was also rejected because

[1] $[X/Y] \equiv \log(X/Y)$–$\log(X/Y)_\odot$. Throughout the text photospheric solar abundances for C and O are taken from Allende Prieto et al. (2001, 2002), for N and Si from Holweger (2000), and for S from Grevesse & Sauval (1998).

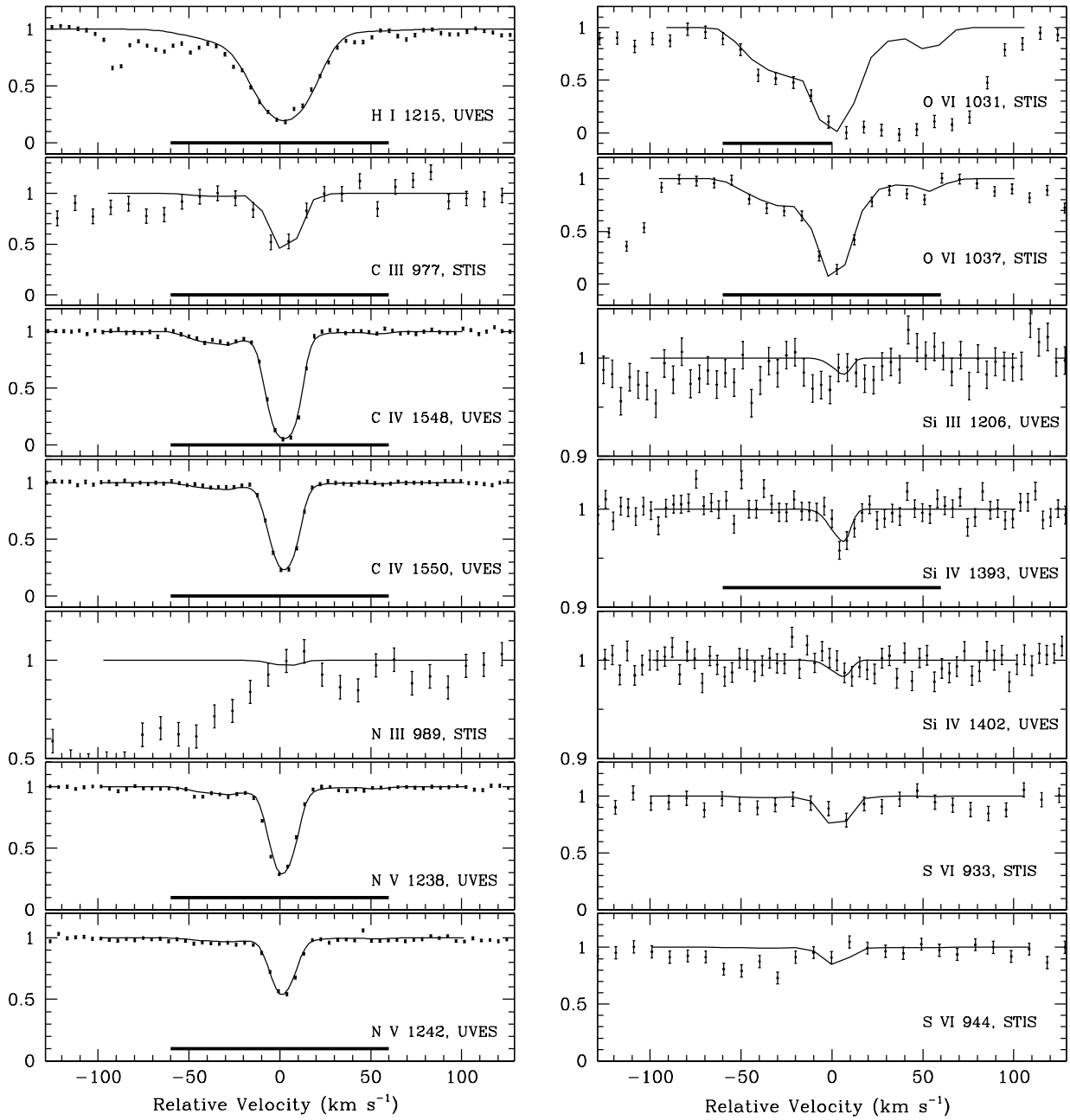

Fig. 4. Hydrogen and metal lines associated with the $z_{abs} = 1.697$ O VI absorption system toward HE 0515–4414 (normalized intensities are shown by dots with 1σ error bars). The zero radial velocity is fixed at $z = 1.6971$. Smooth lines are the synthetic spectra convolved with the corresponding point-spread functions and computed with the physical parameters from Table 1, Col. 8. Bold horizontal lines mark pixels included in the optimization procedure. Spectra obtained with the VLT/UVES and the HST/STIS spectrographs are marked by UVES and STIS, respectively. The normalized $\chi^2_{min} = 1.10$ (the number of degrees of freedom $\nu = 276$).

it produced an anomalously low Si abundance inconsistent with the relative (to solar) abundances of other α-elements O and S. Among the power law continua the optimal fitting was found with $\alpha = -1.5$.

The obtained results are listed in Table 1, Col. 8 and illustrated in Figs. 4 and 5. In Fig. 4, parts of line profiles included in the least-squares minimisation are marked by horizontal lines in the corresponding panels. The synthetic profiles of the N III 989 Å, Si III 1206 Å and S VI 933 Å lines were calculated in a second round using the velocity $v(x)$ and gas density $n_H(x)$ distributions already obtained (see Fig. 5) and the metallicities chosen in such a way that the synthetic spectra did not exceed 1 σ deviations from the observed normalized intensities.

The identification of S VI should be considered, however, with some caution because of the limited *S/N* in the STIS data which prevents a clear detection of the weaker 944 Å component of the S VI doublet. The observed equivalent width of the stronger 933 Å component is $W_{obs} \simeq 52$ mÅ. The STIS

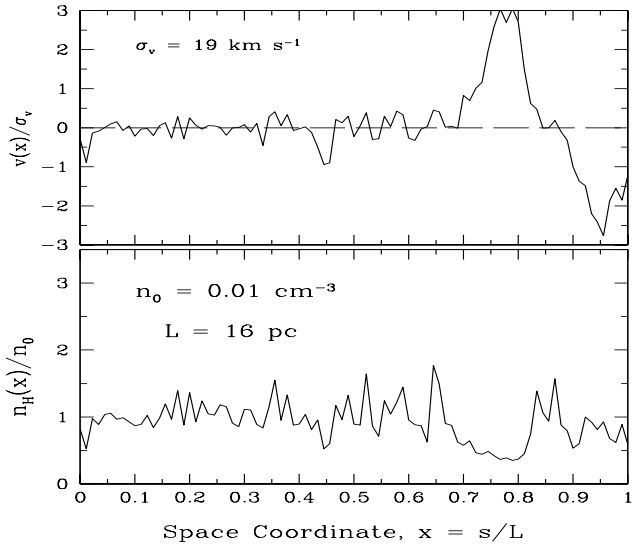

Fig. 5. Computed velocity (upper panel) and gas density (lower panel) distributions along the line of sight within the $z_{\rm abs} = 1.697$ absorber toward HE 05150–4415. Shown are patterns rearranged according to the principle of minimum entropy production rate (Levshakov et al. 2002). The n_0 and L values shown in the lower panel correspond to a limiting case which assumes that the difference $\Delta z_{\rm em-abs}$ is entirely due to cosmological expansion.

data provide the equivalent width detection limit in this spectral range of $\sigma_{\rm lim} \simeq 12$ mÅ if the accuracy of the local continuum fitting δ_c is about 5% and $S/N = 10$. It is seen that formally $W_{\rm obs} > 4\sigma_{\rm lim}$ and thus the absorption feature at the expected position of the S VI 933 Å line is, probably, real. We suggested that this feature may be attributed to S VI and found that the derived sulphur abundance was in line with the abundances of other α-chain elements.

Figure 4 shows that the observed profiles (portions free from blending) are well represented. The red wing of the O VI 1031 Å is partly contaminated by some Lyα forest absorption, but the O VI 1037 Å is well fitted to the observed profile.

A pronounced asymmetry seen in the wings of the C IV, N V, and especially O VI lines is caused by the underdense region with the space coordinates $0.65 \le x \le 1.0$ where a strong velocity gradient is detected (see Fig. 5). This figure also shows no high perturbations in the velocity and density fields along the line of sight between $x = 0$ and $x = 0.65$.

A linear size $L \le 16$ pc was estimated under the assumption that the velocity difference between the QSO and the O VI system is entirely due to the cosmological expansion. If the absorbing cloud has its own significant radial velocity, it could be situated nearer to the emitting region (this will reduce the linear size of the cloud and increase its volumetric density). The size of this system is in line with measurements of other associated systems which show the line of sight extension of order of magnitude from parsecs to tens of parsecs (e.g., Rauch et al. 1999; Papovich et al. 2000; Hamann et al. 2001).

The relative metal abundances measured in this system show almost the solar pattern but the metallicity is about 5 times solar. The total hydrogen column density could be higher and, hence, the general metallicity lower if the QSO continuum revealed some strong emission lines at $\lambda \le 912$ Å. But the observed spectrum of HE 0515–4414 does not show any strong emission in this region (see Reimers et al. 1998). Another possibility to enhance the hydrogen column density could be due to incomplete covering of the continuum source by the absorbing cloud which makes the saturated lines look like unsaturated ones (e.g., Petitjean et al. 1994; Petitjean & Srianand 1999). Obviously it is not the case for the system under study: none of the observed profiles show flattened bottoms and the doublet ratios for the C IV 1548, 1550 Å and N V 1238, 1242 Å pairs are fulfilled perfectly.

Near solar or over solar metallicities are frequently measured in QSO environments (Hamann & Ferland 1999) and in the associated systems (e.g., Petitjean et al. 1994; Savaglio et al. 1997; Hamann et al. 2000; Papovich et al. 2000; Hamann et al. 2001). High metallicity is usually explained by rapid and extensive star formation in the galaxy surrounding the quasar. Extremely high metallicity derived from the $z_{\rm abs} = 1.697$ system suggests its close physical association with the quasar/host galaxy. This system is probably a product of the blowout related to a starburst and/or the onset of quasar activity. In this regard possible implications to the origin of some high velocity clouds (HVCs) will be discussed in Sect. 5.

4.2. O VI absorber at $z_{\rm abs} = 1.674$

The absorption system exhibits hydrogen lines up to Ly-7 and metal ionic transitions C IV and O VI (see Fig. 6). The Doppler widths of the C IV and O VI lines are $\simeq$20 km s^{-1} with $b_{\rm C\,IV}$ slightly lower than $b_{\rm O\,VI}$ (RBHL). This fact and the coexistence of essential amounts of C IV and O VI requires that photoionization play a central role in maintaining the ionization states in this system.

At the positions of the C II 1334 Å and Si II 1260 Å as well as Si IV 1393 Å, and N V 1238 Å clear continuum windows are seen which implies that the system is highly ionized (the C III 977 Å line is completely blended). The O VI 1037 Å is blended, but the stronger 1031 Å component is clear and its profile can be very well fitted to the synthetic spectrum calculated simultaneously with the carbon C IV and hydrogen H I lines.

The Lyα profile has a distinctive shape – flat bottom of the width $\simeq$100 km s^{-1}and pronounced wings extended over 150 km s^{-1}. It is worth noting that similar spectral shape of Lyα has been observed in the $z_{\rm abs} = 4.81$ associated system toward the quasar APM BR J0307–4945 with $z_{\rm em} = 4.753$ (Levshakov et al. 2003a). Such spectral shapes my be formed in the halos of the intervening galaxies with infalling (accretion) or outflowing (galactic wind) gas.

The MCI analysis with the HM spectrum produced results listed in Col. 6 of Table 1. The gas density $n_0 = 8.3 \times 10^{-4}$ cm^{-3}and the linear size $L = 14$ kpc were calculated with $J_{\rm Q} = 2.0 \times 10^{-21}$ erg cm^{-2} s^{-1} Hz^{-1} sr^{-1} as estimated above. This value is 4 times higher as compared with J_{912} at $z = 1.7$ given by HM, i.e. without additional radiation from the quasar the size of the absorber would exceed 50 kpc.

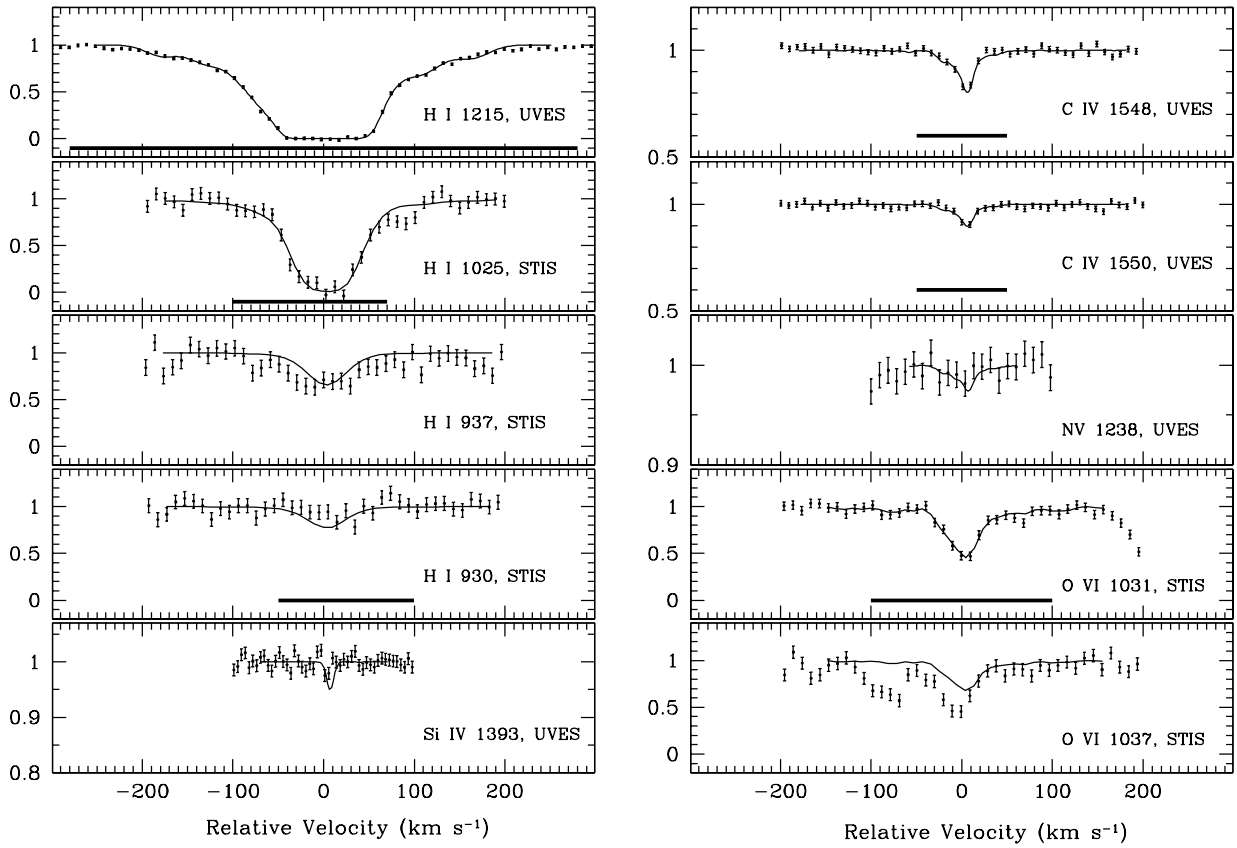

Fig. 6. Same as Fig. 4 but for the $z_{\rm abs} = 1.674$ O VI absorption system. The zero radial velocity is fixed at $z = 1.6736$. The corresponding physical parameters are listed in Table 1, Col. 7. Here $\chi^2_{\rm min} = 0.93$, $\nu = 487$.

Another type of the UV background was also tested. Being shifted at only ≃4000 km s^{-1} from the QSO, the $z_{\rm abs} = 1.674$ system may be directly influenced by the quasar radiation. The results obtained with a power law ionizing continuum ($\alpha = -1.5$, $J_{\rm Q} = 2.0 \times 10^{-21}$ erg cm^{-2} s^{-1} Hz^{-1} sr^{-1}) are shown in Fig. 6, whereas the corresponding physical parameters are given in Col. 7, Table 1.

The measured abundance pattern [log(C/O), log(N/O), and log(O/H)] is similar for both types of the UV background spectra and consistent within the uncertainty range (the accuracy of our $Z_{\rm C}$ and $Z_{\rm O}$ values are about 15% and 25%, respectively) with that observed in the extragalactic H II regions (Henry et al. 2000). The synthetic spectra are also indistinguishable in these two cases. Unfortunately, many elements from the $z_{\rm abs} = 1.674$ system are represented by their upper limits. Besides, we do not observe different ionic transitions of the same element (like C III and C IV, or N III and N V) which could help us to select the most adequate ionizing continuum. However, the relative abundance ratio $[{\rm C/O}] = -0.55 \pm 0.15$ measured for the model with the power law spectrum shows formally a better concordance with the [C/O] values observed in the extragalactic metal-poor H II regions ([C/O] ≃ −0.5) than the ratio $[{\rm C/H}] = -0.72 \pm 0.15$ measured with the HM spectrum. But this uncertainty in the shape of the ionizing spectrum does not hamper the classification of the present system as a metal-poor highly ionized absorber with the linear size of several kiloparsecs.

The question is whether this system is physically associated with the quasar environment or not. The virial mass of the absorber is estimated as $M_{\rm vir} \simeq 10^9\ M_\odot$ and if independent from the QSO, its proper luminosity distance is $D = 12.2\ h_{75}^{-1}$ Mpc. Such masses are comparable to that of dwarf galaxies whereas the distance of ≳10 Mpc is consistent with distances between galaxies. The measured metallicity [C/H] ∼ 1/40 − 1/130 $Z_\odot$ is within the range of metal abundances found in galactic halos. Thus, we may conclude that the most probable origin of the $z_{\rm abs} = 1.674$ absorption system is an external halo of some intervening galaxy located not far from the QSO and directly affected by its radiation.

4.3. O VI absorber at $z_{\rm abs} = 1.602$

There are several unsaturated hydrogen lines and a weak O VI 1031, 1037 Å doublet in this system (see Fig. 7). We also used continuum windows at the expected positions of C III 977 Å, C IV 1548 Å, and N V 1238 Å to constrain the ionization state and metallicity of this system, and a window at the position of Lyγ to control the N(H I) value.

The system was analyzed with the HM spectrum. The results obtained are given in Col. 4, Table 1, the observed and overplotted synthetic spectra are shown in Fig. 7. The volumetric gas density and the linear size of the absorber were estimated for the value of J_{912} given by HM for $z = 1.6$. Since the total number of ions is small, the accuracy of the oxygen

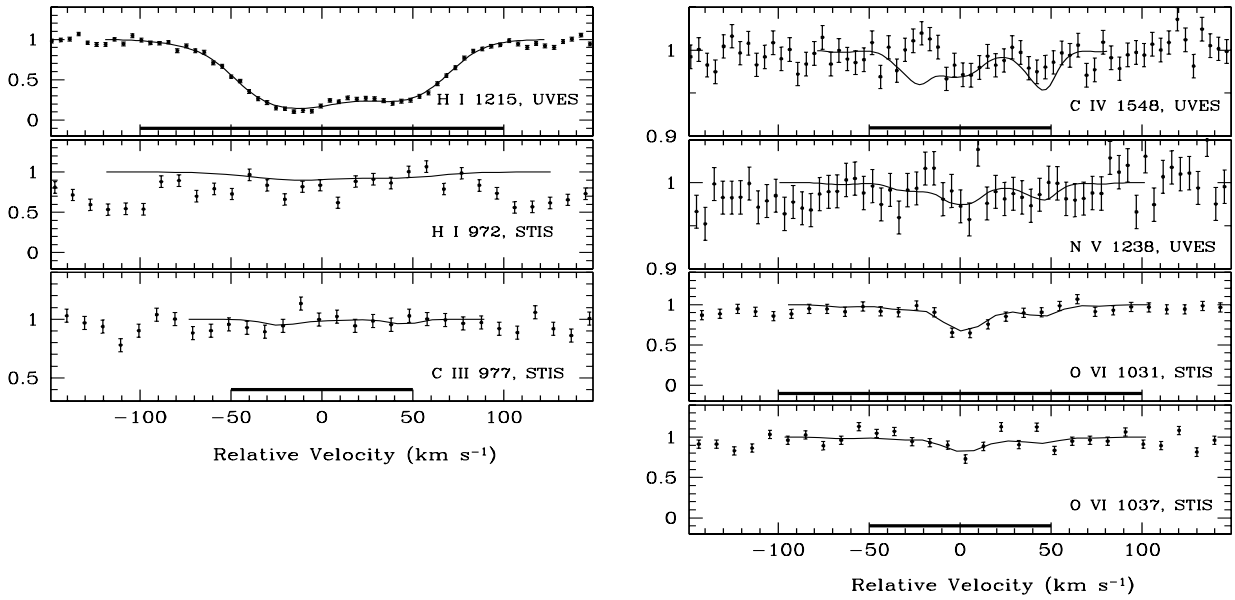

Fig. 7. Same as Fig. 4 but for the $z_{\rm abs} = 1.602$ O VI absorption system. The zero radial velocity is fixed at $z = 1.6019$. The corresponding physical parameters are listed in Table 1, Col. 4. Here $\chi^2_{\rm min} = 1.00$, $\nu = 163$.

abundance estimation is rather low, ∼50%. The accuracy of the column density determinations are about 10% and 20% for N(H I) and N(O VI), respectively.

Here we observe again a low value of the Doppler parameter $b_{\rm O\,VI} = 12.5 \pm 3.6$ km s^{-1} (RBHL) which may indicate that the kinetic temperature is not very high. The system exhibits a complex structure – two strong subcomponents are seen in the hydrogen Lyα profile. The widths of these components are not consistent with temperatures larger than 10^5 K. But the O VI profiles might be caused, in principle, by collisional ionization if one assumes that another wide and shallow Lyα subcomponent is hidden in the spectrum. Since, however, there is no evidence for a broad hydrogen component, it is not possible to carry out any quantitative estimations for this case.

According to the recovered values of the physical parameters (high $U_0 = 0.26$, low $Z \lesssim 1/10\ Z_\odot$, low gas density $n_0 \simeq 1.6 \times 10^{-4}$ cm^{-3}, and the line of sight size $L \simeq 17$ kpc), the $z_{\rm abs} = 1.602$ system may be formed in the external halo of an intervening galaxy. The luminosity distance of $\simeq 38\ h_{75}^{-1}$ Mpc implies that this O VI system is not influenced directly by the QSO radiation.

4.4. O VI absorber at $z_{\rm abs} = 1.385$

This system consists of at least two subcomponents with very different chemical compositions: a metal-rich component at $z_{\rm abs} = 1.3849$ which reveals absorption lines of C III 977 Å, C IV 1548, 1550 Å and O VI 1031 Å (O VI 1037 Å is blended), and a component shifted at $\Delta v \simeq 140$ km s^{-1} and showing no clear metal absorption in the observational range (see Fig. 8). The absorption features seen in the C III panel in Fig. 8 at $\Delta v \lesssim -30$ km s^{-1} and $\Delta v \gtrsim 40$ km s^{-1} belong to the N II λ1084 Å subcomponents from the damped Lyα system at $z_{\rm abs} = 1.15$ (de la Varga et al. 2000). Surprisingly the second component at $\Delta v \simeq 140$ km s^{-1} is much more abundant in neutral hydrogen.

The metal-rich subsystem shows an unsaturated Lyα and no distinguished absorption in Lyβ. The measured neutral hydrogen column density is N(H I) $\simeq 5.3 \times 10^{13}$ cm^{-2} (Table 1, Col. 3). The saturated Lyα and Lyβ lines of the metal-free subsystem give N(H I) $\simeq 1.1 \times 10^{15}$ cm^{-2} and $b = 35.4$ km s^{-1}, that are estimated from the Voigt profile fitting shown by the dotted lines in Fig. 8.

The O VI system at $z_{\rm abs} = 1.385$ was firstly analyzed with the HM spectrum at $z = 1.4$. The obtained physical parameters are listed in Table 1, Col. 3. In Fig. 8, the synthetic profiles (smooth lines) are shown together with the observational data (dots with 1 σ error bars) in a wide radial velocity range to illustrate different metal composition in the metal-rich and metal-free subsystems.

We note that the accuracy of the fit to the blue wing of the Lyα is not sufficiently high. The calculated profile lies slightly over the data points in the range -55 km s$^{-1} \lesssim \Delta v \lesssim -30$ km s^{-1} and under the observed intensities in the range -15 km s$^{-1} \lesssim \Delta v \lesssim 0$ km s^{-1}. However, the shape of the synthetic Lyα profile is fixed by the spectral shapes of the C IV lines which were observed with considerably higher *S/N* and higher spectral resolution. Any attempts to improve the fitting of the blue wing of the Lyα led to distortions in the synthetic C IV profiles inconsistent with the data points. For the same reason the red wing of the Lyα cannot be self-consistently fitted to the model in the range 15 km s$^{-1} \lesssim \Delta v \lesssim 70$ km s^{-1} under the assumption of a constant metallicity across the absorber. If, however, we do observe a strong metallicity gradient, then the fitting of the Lyα may be easily improved assuming an additional metal-free component located at $\Delta v \simeq 30$ km s^{-1}. Higher *S/N* data are required to investigate this spectrum in more detail. Within the present model, we may overestimate the value of N(H I) at $z_{\rm abs} = 1.3849$ by a few percent.

Table 2. Measured H I column densities and upper limits (3 σ) for the metal-free systems toward HE 0515–4414.

Parameter	λ_0, Å	z_{abs} = 1.38601	z_{abs} = 1.49985	z_{abs} = 1.66766	z_{abs} = 1.68064
(1)	(2)	(3)	(4)	(5)	(6)
N(H I), cm^{-2}	Ly$\alpha,\beta,\gamma,\delta,\zeta$	1.1E15	1.7E15	2.7E14	1.8E15
N(C II), cm^{-2}	1334.5	<1.7E12	<1.1E12	<6.0E11	<5.6E11
N(Si II), cm^{-2}	1260.4, 1526.7	<6.7E11	<9.6E11	<7.1E10	<9.0E10
N(Fe II), cm^{-2}	2382.8	<5.0E10	<7.6E10	<5.2E10	<6.7E10
N(C III), cm^{-2}	977.0	<4.6E12	<1.8E12	...	...
N(Si III), cm^{-2}	1206.5	<5.9E11	<8.0E11	<1.2E11	...
N(C IV), cm^{-2}	1548.2, 1550.8	<2.9E11	<3.2E11	<3.0E11	<4.5E11
N(Si IV), cm^{-2}	1393.8, 1402.8	<2.3E11	<2.2E11	<9.7E10	<7.8E10
N(N V), cm^{-2}	1238.8, 1242.8	<7.1E12	<1.8E12	<2.2E12	<1.0E12
N(O VI), cm^{-2}	1031.9, 1037.6	<1.8E13	<4.0E12	<7.5E12	<3.3E13

The measured values of U_0, metallicity, n_0, and T_{kin} are very much alike to those found in the z_{abs} = 2.848 system toward Q0347–3819 (Levshakov et al. 2003a). We consider this similarity as a support for our assumption that these systems may be high-z counterparts of the HVCs observed in the Milky Way halo.

A relatively low ratio of [C/O] = -0.38 ± 0.17 at the measured oxygen abundance of 12 + log(O/H) = 8.65 may, however, indicate that the choice of the HM background was not optimal. We tried to investigate this question by using slightly modified HM spectra. As noted by Fardal et al. (1998), in calculated metagalactic UV spectra the strength of the break at 4 Ryd (which accounts for He II attenuation in intervening clouds) depends strongly on the assumed opacity model at a given redshift. We found that the derived [C/O] ratio is very sensitive to small changes in the value of this decrement at 4 Ryd. For instance, if we modify the HM continuum by decreasing the depth of the break at 4 Ryd by a factor of 1.25 (0.1 dex), then [C/O] = -0.12 ± 0.17 which is in a much better concordance with the measurements in the extragalactic H II regions. The corresponding physical parameters, calculated with this modified HM spectrum, are listed in Table 1, Col. 2 (the accuracy of Z_C and Z_O is about 15% and 40%, respectively).

The choice of the photoionization model for the z_{abs} = 1.385 system can be supported by the same arguments as for the O VI cloud at z_{abs} = 1.674. Namely, we observe $b_{C\,IV}/b_{O\,VI} \simeq 0.6$ (RBHL) as well as a relatively large ratio N(C IV)/N(O VI) $\simeq$ 0.2 which cannot be realized in collisionally ionized gas.

We can also set an upper limit on the metallicity in the metal-free cloud using the estimated limits from Table 2. Because of the blended range at $\Delta v > 50$ km s^{-1}, we are not able to judge whether a C III λ977 Å absorption is present at $\Delta v \simeq 150$ km s^{-1} or not. If we attribute the absorption feature at $\Delta v \simeq 150$ km s^{-1} to the C III line, then it would require a high $\Upsilon_{C\,III}/\Upsilon_{C\,IV}$ ratio and, hence, a low ionization parameter, $U_0 \sim 10^{-3}$–10^{-2}, which gives the gas number density of $n_0 \sim 10^{-2}$–10^{-3} cm^{-3} and a cloud size from 10s to 100s of pc, assuming the HM background spectrum. The corresponding carbon abundance limit would be [C/H] <−1.5 and <−2.5. However, the O VI cloud at $\Delta v = 0$ km s^{-1} has the linear size of ∼2 kpc which is too low for a cloud to be in space on its own, so both systems are probably physically connected. Taking into account that the O VI system exhibits a high metallicity, the structure of two clouds when a metal-poor component ($\Delta v = 150$ km s^{-1}) is surrounded and pressure confined by a hot metal-rich gas ($\Delta v = 0$ km s^{-1}) seems to be quite unphysical. A more plausible interpretation of the observed spectrum is that the line of sight intersects some peculiar object (like a star burst region, a superbuble, an infalling shell fragment etc.) which is metal-enriched and embedded in a metal-deficit halo of an intervening galaxy. This metal-poor gas is likely to be photoionized since the estimated Doppler parameter $b_H = 35.4$ km s^{-1} implies $T \leq 7.4\times10^4$ K. If we assume that the incident UV radiation has the HM spectrum at $z = 1.4$ and the ionization state in the metal-poor system is approximately the same as in the nearest metal-rich system (i.e., $U_0 \gtrsim 0.1$), then for a constant gas density ($\sigma_y = 0$) the conservative limits on the total oxygen and carbon column densities are N(O) < 1.8×10^{14} cm^{-2} and N(C) < 2.0×10^{12} cm^{-2}, while the total hydrogen column density is N(H) = 4.4×10^{19} cm^{-2}. Under this assumption, we obtain [O/H] < −2.0 and [C/H] < −3.7 and the linear size of this absorber $L \gtrsim 90$ kpc. The upper limits on the metal abundances may be increased by about 0.3–0.5 dex and the linear size decreased by several times, if the density is inhomogeneous (e.g., $\sigma_y \sim 1$).

The metallicity of the pristine gas at the level 10^{-4} to $10^{-3} Z_\odot$ can be already produced by the first Population III stars (e.g., Nakamura & Umemura 2001). At face value, our estimations suggest that this metal-free system can indeed consists of primordial gas.

4.5. O VI absorber at z_{abs} = 1.667

This new O VI system identified in the present study reveals the striking similarity to the preceding O VI absorber at z_{abs} = 1.385. Two close subcomponents with very different chemical compositions are observed: a metal-rich component at z_{abs} = 1.66695 showing absorption lines of C IV 1548 Å, N V 1238 Å

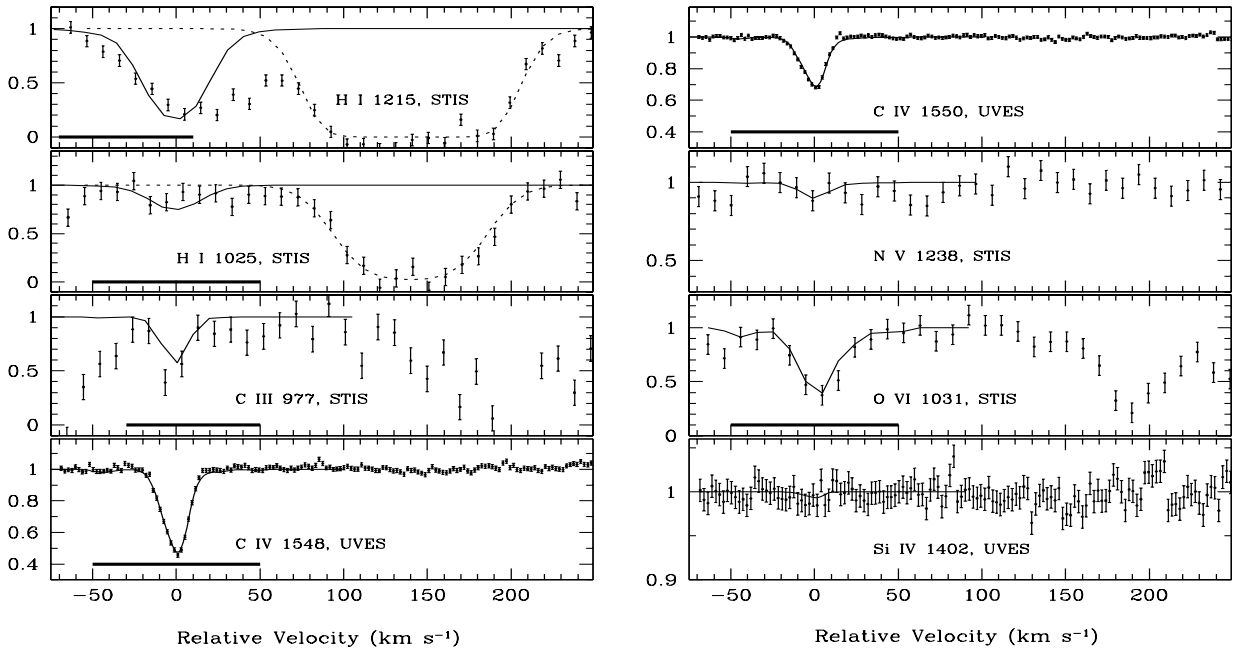

Fig. 8. Same as Fig. 4 but for the $z_{\rm abs} = 1.385$ O VI absorption system. The zero radial velocity is fixed at $z = 1.3849$. The corresponding physical parameters are listed in Table 1, Col. 3. Here $\chi^2_{\rm min} = 1.20$, $\nu = 123$. In addition to the $z_{\rm abs} = 1.385$ system, hydrogen absorption seen at $\Delta v \simeq 140$ km s^{-1} is shown by dotted lines. No metals are detected at this Δv. A wide absorption feature in the O VI panel at $\Delta v > 130$ km s^{-1} is due to the Fe II λ1144 Å line from the damped Lyα system at $z_{\rm abs} = 1.15$ (de la Varga et al. 2000), whereas absorption features in the C III panel at $\Delta v \lesssim -30$ km s^{-1} and $\Delta v \gtrsim 40$ km s^{-1} are caused by the N II λ1084 Å absorption components from the $z_{\rm abs} = 1.15$ system.

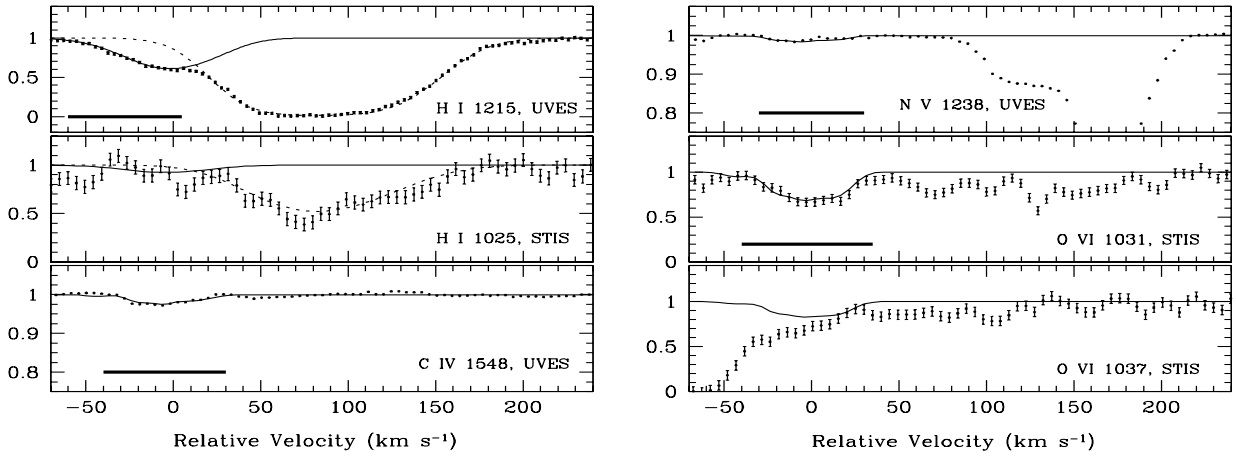

Fig. 9. Same as Fig. 4 but for the $z_{\rm abs} = 1.667$ O VI absorption system. The zero radial velocity is fixed at $z = 1.66695$. The corresponding physical parameters are listed in Table 1, Col. 5. Here $\chi^2_{\rm min} = 0.91$, $\nu = 99$. In addition to the $z_{\rm abs} = 1.667$ system, hydrogen absorption seen at $\Delta v \simeq 80$ km s^{-1} is shown by dotted lines. No metals are detected at this Δv. The absorption features in the range $\Delta v \simeq 125{-}200$ km s^{-1} in the O VI 1031 Å panel are caused by the C I 1280 Å lines from the damped Lyα system at $z_{\rm abs} = 1.15$ (de la Varga et al. 2000), whereas features at $\Delta v \simeq 70$ km s^{-1} and 100 km s^{-1} are unidentified.

and O VI 1031 Å (C IV 1550 Å and N V 1242 Å are too weak, and O VI 1037 Å is partly blended as seeing in Fig. 9), and a component shifted at $\Delta v \simeq 80$ km s^{-1} without any distinctive metal absorption both in low (C II, Si II, Fe II) and high (Si III, Si IV, C IV, N V, O VI) ionic transitions. The C III line is blended with strong Lyγ absorption from the metal-free system at $z_{\rm abs} = 1.681$. The second component shows again considerably higher neutral hydrogen column density, N(H I) $\simeq 2.7 \times 10^{14}$ cm^{-2} (Table 2, Col. 5) as compared to the metal-rich system with N(H I) $\simeq 2.2 \times 10^{13}$ cm^{-2} (Table 1, Col. 5).

The observed Lyα and Lyβ profiles are shown in Fig. 9 where the overplotted solid lines are the MCI solutions and the dotted lines correspond to the Voigt profiles (centered at $\Delta v = 67.6$ km s^{-1} and 100.0 km s^{-1}) which were used to estimate the total N(H I) in the metal-free component.

The metal line profiles are rather wide and shallow (shown by dots in Fig. 9 are their profiles filtered with a median filter to increase the contrast) and exhibit non-Gaussian shapes. Their apparent widths are $FWHM_{\rm C\,IV} \simeq FWHM_{\rm O\,VI} \simeq 45 \pm 3$ km s^{-1} (N V is too weak to provide an accurate estimation), and that

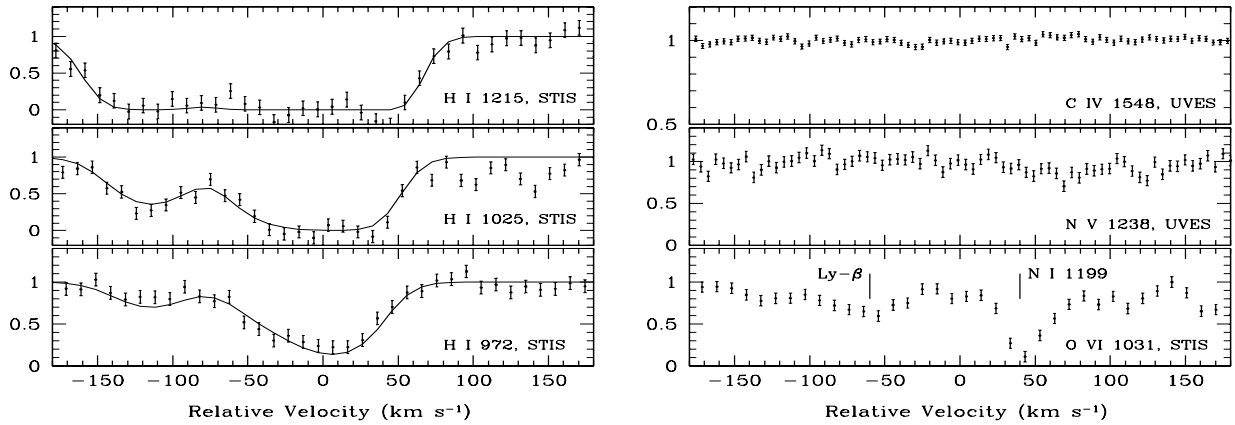

Fig. 10. An example of the metal-free Lyα system at $z_{\rm abs} = 1.500$ toward HE 0515–414. The zero radial velocity is fixed at $z = 1.499854$. Smooth lines are the combined synthetic spectra of three subcomponents centered at $\Delta v = -114.5$, -27.6, and 11.0 km s^{-1} and convolved with the STIS point-spread function. The cental components show the total N(H I) $\simeq 1.8 \times 10^{15}$ cm^{-2}. In panel O VI, the absorption features at $\Delta v \simeq -60$ km s^{-1} and $\simeq 40$ km s^{-1} are due to the Lyβ line from the $z_{\rm abs} = 1.515$ system and to the N I 1199 Å line from the damped Lyα system at $z_{\rm abs} = 1.15$ (de la Varga et al. 2000).

of the hydrogen component at $\Delta v = 0$ km s^{-1} is $FWHM_{\rm H\,I} \simeq 56 \pm 3$ km s^{-1}. Although the widths of C IV and O VI allow formally for the temperature $T_{\rm kin} > 10^5$ K, their collisional ionization should nevertheless be ruled out because the hydrogen Lyα line is not wide enough and its profile cannot be extended over $|\Delta v| > 50$ km s^{-1} due to high *S/N* in both hydrogen ($\Delta v < -50$ km s^{-1}) and carbon ($\Delta v > 50$ km s^{-1}) lines. On the contrary, the observed profiles of these hydrogen and metal lines can be well described assuming turbulent broadening and photoionization by a single power law continuum $J_\nu \propto \nu^{-1.5}$ normalized at 1 Ryd to $J_{\rm Q} = 2 \times 10^{-21}$ erg cm^{-2} s^{-1} Hz^{-1} sr^{-1}. The corresponding physical parameters are given in Table 1, Col. 5. The accuracy of the estimated metallicities is not high ($\simeq \pm 0.2$ dex) since carbon and nitrogen lines are very weak and the signal-to-noise ratio in the O VI data is rather low. But the most probable values of [C/O] $\simeq -0.1$ and [N/O] $\simeq -0.4$ are in line with the abundances measured in the extragalactic H II regions with a relatively high metallicity 12 + log(O/H) $\simeq 8.2$ (cf., Henry et al. 2000; Centurión et al. 2003).

The obtained metallicity $Z \simeq 1/3 Z_\odot$, number density $n_0 \simeq 4 \times 10^{-4}$ cm^{-3} and the linear size $L \simeq 900$ pc are typical for the HVCs observed in the Milky Way. We suggest that this system may be embedded in an external halo of some galaxy at $z_{\rm abs} \simeq 1.667$. The wide and shallow metal lines may be explained if the metal-enriched cloud is driven away by an outflow similar to that observed in the wings of the Lyα line from the neighbour system at $z_{\rm abs} = 1.674$. Using the mean ionization parameter $U_0 \gtrsim 0.2$ for the metal-free system at $\Delta v \simeq 80$ km s^{-1} and assuming that it is photoionized by the same background spectrum (i.e. $J_\nu \propto \nu^{-1.5}$), we obtain a conservative upper limit for the metal abundances in this galactic halo: [C/H] < -2.4 and [O/H] < -2.5 (upper limits on the column densities from Table 2, Col. 5 are used).

Thus, both O VI systems, that at $z_{\rm abs} = 1.385$ and $z_{\rm abs} = 1.667$, show a strong metallicity gradient $|{\rm d[C/H]/d}v| > 0.02$ (km s^{-1})$^{-1}$, which may imply that the metal enrichment of the metagalactic medium was very inhomogeneous in space and time. Lyα systems described in the next section support this conclusion.

4.6. Metal-free systems at $z_{\rm abs} = 1.500$ and 1.681

The metal-free absorbers showing a moderate neutral hydrogen column density of N(H I) $\sim 10^{15}$ cm^{-2} are not rare in QSO spectra. For instance, in HE 0515–4414 we identified another two systems at $z_{\rm abs} = 1.500$ and 1.681 with, respectively, N(H I) $\simeq 1.7 \times 10^{15}$ and 1.8×10^{15} cm^{-2} (the uncertainty is about 6% for both cases) without any clear metal lines in the observational wavelength range.

Figure 10 represents the H I Lyα, Lyβ, and Lyγ lines, and the continuum windows at the expected positions of the C IV 1548 Å, N V 1238 Å, and O VI 1031 Å lines from the former system. We find that three components centered at $\Delta v = -114.5$, -27.6, and 11.0 km s^{-1} describe adequately the hydrogen absorption with N(H I) $= 2.7 \times 10^{14}$, 6.2×10^{14}, and 1.2×10^{15} cm^{-2}, and $b = 31$, 34, and 29 km s^{-1}, respectively (the combined synthetic spectra are shown by the smooth lines).

In Fig. 11, another metal-free system is shown. Here three hydrogen components centered at $\Delta v = -97.0$, -34.0, and 0.0 km s^{-1} with $b = 54.7$, 48.0, and 22.0 km s^{-1} and N(H I) $= 1.6 \times 10^{13}$, 5.25×10^{14}, and 1.13×10^{15} cm^{-2}, respectively, fit perfectly the observed hydrogen profiles. However, we do not detect any absorption in C IV 1548 Å, N V 1238 Å, and O VI 1031 Å lines or in the low ions listed in Table 2, Cols. 4 and 6. To deduce the upper limits on the metallicity for both systems, we applied the same assumptions as for the metal-free systems previously described, i.e. photoionization by either the HM spectrum at $z = 1.5$ or by the power law spectrum ($\nu = -1.5$) at $z = 1.68$, the mean ionization parameter $U_0 \lesssim 0.1$ and the upper limits on the column densities from Table 2. The estimated limits on the metal abundances are [C/H] < -4.0, [O/H] < -3.0 ($z_{\rm abs} = 1.500$) and [C/H] < -3.0, [O/H] < -2.5 ($z_{\rm abs} = 1.681$), assuming constant density.

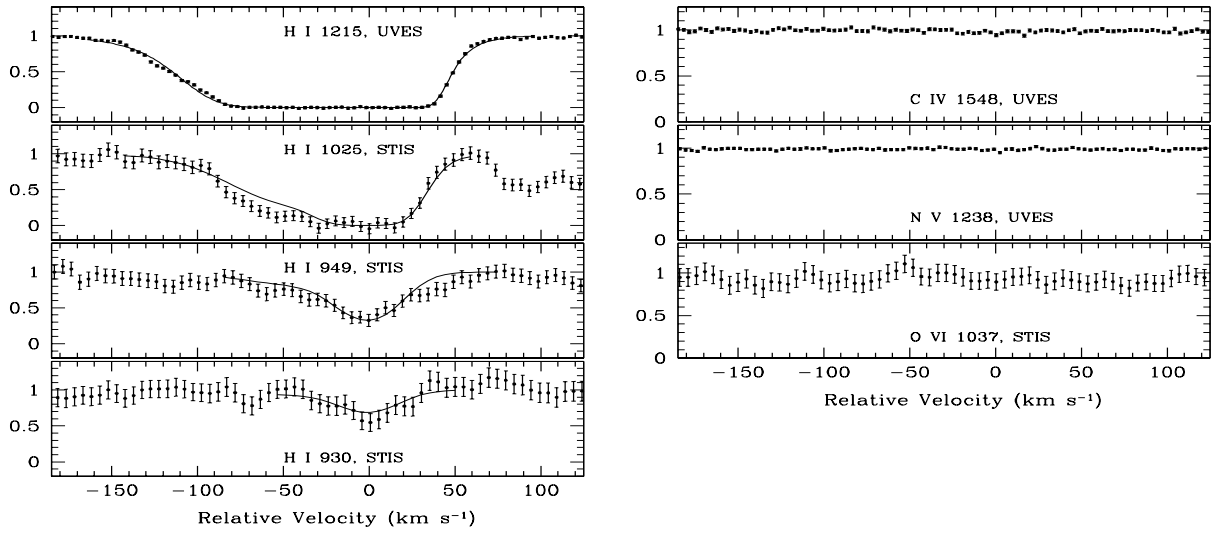

Fig. 11. Same as Fig. 10 but for the metal-free Lyα system at $z_{abs} = 1.681$. The zero radial velocity is fixed at $z = 1.68064$. Smooth lines are the combined synthetic spectra of three subcomponents centered at $\Delta v = -97.0$, -34.0, and 0.0 km s^{-1} and convolved with the UVES and STIS point-spread functions. The total neutral hydrogen column density is $N(\mathrm{H\,I}) \simeq 1.7 \times 10^{15}$ cm^{-2}. In panel H I 1025 Å, the portion of the Lyβ line at $\Delta v \simeq -60$ km s^{-1}is probably contaminated by the Lyα forest.

We note that extremely low metal abundances are detected not only in typical Lyα forest clouds with $N(\mathrm{H\,I}) \sim 10^{15}$ cm^{-2}, but also in the so-called Lyman-limit systems (LLSs) having $N(\mathrm{H\,I}) \gtrsim 10^{17}$ cm^{-2}. For instance, in the LLS at $z_{abs} = 2.917$ with $N(\mathrm{H\,I}) = 3.2 \times 10^{17}$ cm^{-2}, the carbon abundance at the level of $\simeq$0.001 $Z_\odot$ was recently measured (Levshakov et al. 2003b).

5. Discussion

We detected no prominent imprints of hot ($T_{kin} > 10^5$ K), collisionally ionized gas in the analyzed O VI systems. All of them can be described self-consistently under the assumption of photoionization only.

Our analysis has shown that the O VI absorbers toward the QSO HE 0515–4414 originate in different environments: the $z_{abs} = 1.697$ system is likely to be physically associated with the QSO/host galaxy, two systems – that at $z_{abs} = 1.674$ and 1.602 – are formed in a smoothly distributed gas in the outer parts of the intervening galaxy halos, whereas the $z_{abs} = 1.385$ and $z_{abs} = 1.667$ absorbers are HVC-type clouds embedded in galaxy halos of an extremely low metallicity ([C/H] < -2.5).

The presented O VI systems demonstrate a wide range of metal abundances: $-1.6 <$ [C/H] < 0.6. Moreover, we detected four systems with $N(\mathrm{H\,I}) \sim 10^{15}$ cm^{-2} which do not show any metal transitions in the observational wavelength range.

These facts imply that our sample of the O VI absorbers does not trace the "warm-hot" gas indicating that its fraction is probably negligible between $z = 1.38$ and $z = 1.7$. Another output is that the present sample cannot be used for the estimation of the cosmological mass density of metals and baryons since the analyzed O VI systems are very heterogeneous and do not allow to make estimations of the mean characteristics of the O VI-bearing gas in general. However, just this diversity of the considered O VI systems leads to the important conclusions concerning the mechanisms of the metal enrichment of the IGM.

The most metal-rich system at $z_{abs} = 1.697$ is an associated system with metallicity of ~5 times solar. As mentioned in Sect. 4.1, such high over solar abundances are usually observed in quasar broad emission line regions. For example, the metallicity of $Z \sim 2\ Z_\odot$ was measured in the $z_{em} = 4.16$ QSO BR 2248–1248 (Warner et al. 2002) and the metallicities of $Z \sim 4\ Z_\odot$ were detected in the spectra of 11 high redshift QSOs ($3.9 \lesssim z \lesssim 5.0$) by Dietrich et al. (2003).

According to galactic chemical evolution models, high metal abundances in the gaseous environments near QSOs are accumulated over a period of ~1 Gyr before the onset of quasar activity (e.g., Matteucci & Padovani 1993; Hamann & Ferland 2000; Romano et al. 2002). A galactic wind may be triggered at the point of the quasar's "turn on" due to the combined effect of QSO and stars. Calculations show that the more massive galactic nuclei are, the shorter is time interval between the onset of the star formation and the peak of the QSO activity (e.g., Monaco et al. 2000).

The mass of the central source of the quasar HE 0515–4414 can be estimated from its luminosity $\mathcal{L}_Q \simeq 2.5 \times 10^{47}$ erg s^{-1} = $6.5 \times 10^{13}\ \mathcal{L}_\odot$. Since it is the brightest QSO, we can assume that its luminosity $\mathcal{L}_Q$ is close to the Eddington limit $\mathcal{L}_E = 1.3 \times 10^{38}(M_Q/M_\odot)$ erg s^{-1}, and thus $M_Q \simeq 2 \times 10^9\ M_\odot$.

The fact that the ionization state of this metal-rich O VI system is maintained by a single power law spectrum $J_\nu \propto \nu^{-1.5}$ implies that the gas between the quasar and the absorbing cloud is highly ionized since the incident UV continuum is not blocked by hydrogen and helium absorption.

A quasar with the luminosity of $6.5 \times 10^{13}\ \mathcal{L}_\odot$ and the ionizing continuum $\propto \nu^{-1.5}$ can essentially ionize gas in a radius of about 1.1 Mpc, assuming $n_H = 0.01$ cm^{-3} and the relative helium abundance (by number) of 10%. So, the distance between the O VI cloud and the QSO nucleus is to be $R_{cl} \lesssim 1$ Mpc. If the gas in this cloud has been enriched by heavy elements synthesised by earlier ($\Delta t \sim 1$ Gyr) star formation episode after which the cloud was blown out into the outer zone of the

galactic halo, then the mean velocity of the outflow should be $R_{\rm cl}/\Delta t \sim 1000$ km s^{-1}, which is comparable to the observed velocity difference $\Delta v_{\rm em-abs}$. An outflow speed as high as 1000 km s^{-1} has been observed in the Lyman break galaxy MS 1512–cB58 at $z = 2.7276$ which is undergoing active star formation (Pettini et al. 2002).

If the O VI system is located at 1 Mpc from the QSO, then its linear size L and the mean gas density n_0 should be scaled by a factor of 4.5^2 as compared to the values from Table 1, Col. 7, giving $L \simeq 0.8$ pc and $n_0 \simeq 0.2$ cm^{-3}. Thus, the $z_{\rm abs} = 1.697$ system may very well be an example of a thin shell or a fragment of a superbubble whose expansion is probably caused by a cumulative effect of supernova and the quasar activity. Such metal-rich outflowing gas is supposed to give rise to some HVCs observed in the Milky Way halo (Bregman 1980; Wakker 2001).

Other metal-rich O VI systems at $z_{\rm abs} = 1.385$ ($Z \sim 1/3\ Z_\odot$, $L \simeq 2$ kpc) and at $z_{\rm abs} = 1.667$ ($Z \sim 1/3\ Z_\odot$, $L \simeq 0.9$ kpc) may be produced by a mechanism known as a galactic fountain (Bregman 1980): gas contaminated by heavy elements arises from the inner region of an intervening galaxy and condenses into a cloud within the halo. After formation, the cloud cools and falls back toward the galaxy center. This mechanism was suggested to explain the origin of the high-metallicity HVCs in the Milky Way.

We can assume that the galactic fountain also functions in distant galaxies. In our case we observe extremely metal-poor halos ([C/H] < -3) which means that star formation processes were not very powerful and therefore the mass of the host galaxy was not, probably, very high. Metal-free environments can also indicate that the HVC is situated in an external part of the halo, which again could be possible only if the gravitational potential of the galaxy was rather low. However, we cannot exclude the possibility that the origin of these O VI clouds is extragalactic. For some galactic HVCs there are indications that they are located at typical distances from the Milky Way of up to 1 Mpc and currently falling into the Local Group (e.g., Blitz et al. 1999). It was shown above that a superbubble fragment like the $z_{\rm abs} = 1.697$ cloud can be blown away from the host galaxy to the distance of ∼1 Mpc. This distance is large enough for a fragment to become a "loose" cosmic object which eventually can be captured by an encountered galaxy.

In the redshift interval from $z = 1.385$ to $z = 1.697$ we have found four metal-free systems at $z_{\rm abs} = 1.385$, 1.500, 1.667, and 1.681 which lie among five metal-rich systems at $z_{\rm abs} = 1.385$, 1.602, 1.667, 1.674, and 1.697. All metal-free systems reveal rather high neutral hydrogen column densities: 1.8×10^{15} cm^{-2} ($z_{\rm abs} = 1.500$), 1.7×10^{15} cm^{-2} ($z_{\rm abs} = 1.681$), 1.1×10^{15} cm^{-2} ($z_{\rm abs} = 1.385$), and 2.7×10^{14} cm^{-2} ($z_{\rm abs} = 1.667$). Taking this into account we may conclude that our results favour in situ enrichment scenarios which were proposed in a number of recent publications (see, e.g., Scannapieco et al. 2002 and references therein).

6. Summary

We have deduced the physical properties of the five O VI systems and four Lyα metal-free systems in the range $\Delta z = 1.385$–1.697 toward HE 0515–4414. The main conclusions are as follows:

1. All O VI systems can be self-consistently described under the assumption of photoionization equilibrium only. This implies that the fraction of shock-heated hot gas with temperature $T_{\rm kin} > 10^5$ K is negligible in these systems.
2. The analyzed O VI systems belong to a *heterogeneous* population which is formed by at least three groups of absorbers: (*i*) gas in a thin shell of a superbubble associated with the QSO/host galaxy (O VI at $z_{\rm abs} = 1.697$); (*ii*) extended low metallicity gas halos of distant galaxies (O VI at $z_{\rm abs} = 1.674$ and 1.602); and (*iii*) metal-enriched gas arising from the inner galactic regions or falling into the external galactic halo (O VI at $z_{\rm abs} = 1.385$ and 1.667).
3. Only a power law type spectrum of the ionizing UV radiation is consistent with the observed sample of metal lines from the associated $z_{\rm abs} = 1.697$ system. The optimal fitting was found with the spectral index $\alpha = -1.5$. The measured metal abundances are about 5 times solar, and the metallicity pattern is solar. The system, located at ∼1 Mpc from the QSO, completely covers the continuum source. The line-of-sight size of the system is $L \simeq 0.8$–16 pc.
4. The absorption systems at $z_{\rm abs} = 1.385$ and 1.667 show characteristics very similar to that observed in metal-enriched HVCs in the Milky Way. These systems can be interpreted as high-redshift counterparts of galactic HVCs.
5. An important outcome of our study is that Lyα absorbers are utterly inhomogeneous in metal abundances. Upper limits on metal contents at the extremely low level of $Z < 10^{-3}\ Z_\odot$ were set for three systems with N(H I) ∼ 10^{15} cm^{-2}.

Acknowledgements. S.A.L. gratefully acknowledges the hospitality of Hamburger Sternwarte, Universität Hamburg. We thank our referee for helpful comments. The analysis of the HST data has been supported by the Verbundforschung of the BMBF/DLR under grant No. 50 OR 0203. The work of S.A.L. and I.I.A. is supported in part by the RFBR grant No. 03-02-17522.

References

Allende Prieto, C., Lambert, D. L., & Asplund, M. 2001, ApJ, 556, L63
Allende Prieto, C., Lambert, D. L., & Asplund, M. 2002, ApJ, 573, L137
Blitz, L., Spergel, D. N., Teuben, P. J., Hartmann, D., & Burton, W. B. 1999, ApJ, 514, 818
Bregman, J. N. 1980, ApJ, 236, 577
Carswell, B., Schaye, J., & Kim, T.-S. 2002, ApJ, 578, 43
Cen, R., & Ostriker, J. P. 1999, ApJ, 514, 1
Centurión, M., Molaro, P., Vladilo, G., et al. 2003, A&A, 403, 55
Davé, R., Cen, R., Ostriker, J. P., et al. 2001, ApJ, 552, 473
de la Varga, A., Reimers, D., Tytler, D., Barlow, T., & Burles, S. 2000, A&A, 363, 69
Dietrich, M., Appenzeller, I., Hamann, F., et al. 2003, A&A, 398, 891
Fardal, M. A., Giroux, M. L., & Shull, M. 1998, AJ, 115, 2206
Ferland, G. J. 1997, A Brief Introduction to Cloudy (Internal Rep., Lexington: Univ. Kentucky)
Grevesse, N., & Sauval, A. J. 1998, Space Sci. Rev., 85, 161
Haardt, F., & Madau, P. 1996, ApJ, 461, 20 [HM]

Hamann, F., & Ferland, G. 1999, ARA&A, 37, 487
Hamann, F. W., Netzer, H., & Shields, J. C. 2000, ApJ, 536, 101
Hamann, F. W., Barlow, T. A., Chaffee, F. H., Foltz, C. B., & Weymann, R. J. 2001, ApJ, 550, 142
Henry, R. B. C., Edmunds, M. G., & Köppen, J. 2000, ApJ, 541, 660
Henry, R. B. C., & Worthey, G. 1999, PASP, 111, 919
Holweger, H. 2001, in Solar and Galactic Composition, ed. R. F. Wimmer-Schweingruber, AIP Conf. Proc., 598, 23
Kriss, G. A., Shull, J. M., Oegerle, W., et al. 2001, Science, 293, 1112
Levshakov, S. A., Chaffee, F. H., Foltz, C. B., & Black, J. H. 1992, A&A, 262, 385
Levshakov, S. A., Agafonova, I. I., & Kegel, W. H. 2000, A&A, 360, 833 [LAK]
Levshakov, S. A., Agafonova, I. I., Centurión, M., & Mazets, I. E. 2002, A&A, 383, 813
Levshakov, S. A., Agafonova, I. I., D'Odorico, S., Wolfe, A. M., & Dessauges-Zavadsky, M. 2003a, ApJ, 582, 596
Levshakov, S. A., Agafonova, I. I., Centurión, M., & Molaro, P. 2003b, A&A, 397, 851
Madau, P., Ferrara, A., & Rees, M. J. 2001, ApJ, 555, 92
Mathews, W. G., & Ferland, G. J. 1987, ApJ, 323, 456 [MF]
Matteucci, F., & Padovani, P. 1993, ApJ, 419, 485
Monaco, P., Salucci, P., & Danese, L. 2000, MNRAS, 311, 279
Morton, D. C. 1991, ApJS, 77, 119
Nakamura, F., & Umemura, M. 2001, ApJ, 548, 19
Papovich, C., Norman, C. A., Bowen, D. V., et al. 2000, ApJ, 531, 654
Petitjean, P., Rauch, M., & Carswell, R. F. 1994, A&A, 291, 29
Petitjean, P., & Srianand, R. 1999, A&A, 345, 73
Pettini, M., Rix, S. A., Steidel, C. C., et al. 2002, ApJ, 569, 742
Rauch, M., Sargent, W. L. W., & Barlow, T. A. 1999, ApJ, 515, 500
Reimers, D., Köhler, S., Hagen, H.-J., & Wisotzki, L. 1998, in Proceed. of the Conference Ultraviolet Astrophysics, Beyond the IUE Final Archive, Sevilla, Spain, 11–14 November 1997, ESA SP-413
Reimers, D., Köhler, S., Wisotzki, L., et al. 1997, A&A, 327, 890
Reimers, D., Baade, R., Hagen, H.-J., & Lopez, S. 2001, A&A, 374, 871
Romano, D., Silva, L., Matteucci, F., & Danese, L. 2002, MNRAS, 334, 444
Savaglio, S., Cristiani, S., D'Odorico, S., et al. 1997, A&A, 318, 347
Scannapieco, E., Ferrara, A., & Madau, P. 2002, ApJ, 574, 590
Smette, A., Heap, S. R., Williger, G. M., et al. 2002, ApJ, 564, 542
Spitzer, L. Jr. 1978, Physical Processes in the Interstellar Medium (New York: Wiley-Interscience)
Spitzer, L. Jr., & Fitzpatrick, E. L. 1993, ApJ, 409, 299
Sutherland, R. S., & Dopita, M. A. 1993, ApJS, 88, 253
Tripp, T. M., Savage, B. D., & Jenkins, E. B. 2000, ApJ, 534, L1
Wakker, B. P. 2001, ApJS, 136, 463
Warner, C., Hamann, F., Shields, J. C., et al. 2002, ApJ, 567, 68